

Diffraction manipulation by four-wave mixing

Itay Katzir^{1,*}, Amiram Ron¹, and Ofer Firstenberg²

¹*Department of Physics, Technion-Israel Institute of Technology, Haifa 32000, Israel*

²*Department of Physics of Complex Systems, Weizmann Institute of Science, Rehovot 76100, Israel*

[*itaykatzir@gmail.com](mailto:itaykatzir@gmail.com)

Abstract: We suggest a scheme to manipulate paraxial diffraction by utilizing the dependency of a four-wave mixing process on the relative angle between the light fields. A microscopic model for four-wave mixing in a Λ -type level structure is introduced and compared to recent experimental data. We show that images with feature size as low as $10\ \mu\text{m}$ can propagate with very little or even negative diffraction. The mechanism is completely different from that conserving the shape of spatial solitons in nonlinear media, as here diffraction is suppressed for arbitrary spatial profiles. At the same time, the gain inherent to the nonlinear process prevents loss and allows for operating at high optical depths. Our scheme does not rely on atomic motion and is thus applicable to both gaseous and solid media.

© 2024 Optical Society of America

OCIS codes: (020.1670) Coherent optical effects; (050.1940) Diffraction; (190.4380) Nonlinear optics, four-wave mixing.

References and links

1. J. Durnin, "Exact solutions for nondiffracting beams. i. the scalar theory," *J. Opt. Soc. Am. A* **4**, 651 (1987).
2. R. Kapoor and G. S. Agarwal, "Theory of electromagnetically induced waveguides," *Phys. Rev. A* **61**, 053818 (2000).
3. A. G. Truscott, M. E. J. Friese, N. R. Heckenberg, and H. Rubinsztein-Dunlop, "Optically written waveguide in an atomic vapor," *Phys. Rev. Lett.* **82**, 1438–1441 (1999).
4. J. Cheng and S. Han, "Electromagnetically induced self-imaging," *Opt. Lett.* **32**, 1162–1164 (2007).
5. O. Firstenberg, M. Shuker, N. Davidson, and A. Ron, "Elimination of the diffraction of arbitrary images imprinted on slow light," *Phys. Rev. Lett.* **102**, 043601 (2009).
6. O. Firstenberg, P. London, M. Shuker, A. Ron, and N. Davidson, "Elimination, reversal and directional bias of optical diffraction," *Nat. Phys.* **5**, 665–668 (2009).
7. M. Fleischhauer, A. Imamoglu, and J. P. Marangos, "Electromagnetically induced transparency: Optics in coherent media," *Rev. Mod. Phys.* **77**, 633 (2005).
8. R. R. Moseley, S. Shepherd, D. J. Fulton, B. D. Sinclair, and M. H. Dunn, "Spatial consequences of electromagnetically induced transparency: Observation of electromagnetically induced focusing," *Phys. Rev. Lett.* **74**, 670–673 (1995).
9. M. Mitsunaga, M. Yamashita, and H. Inoue, "Absorption imaging of electromagnetically induced transparency in cold sodium atoms," *Phys. Rev. A* **62**, 013817 (2000).
10. D. Bortman-Arbiv, A. D. Wilson-Gordon, and H. Friedmann, "Induced optical spatial solitons," *Phys. Rev. A* **58**, R3403–R3406 (1998).
11. A. Andre, M. Bajcsy, A. S. Zibrov, and M. D. Lukin, "Nonlinear optics with stationary pulses of light," *Phys. Rev. Lett.* **94**, 063902 (2005).
12. J. Cheng, S. Han, and Y. Yan, "Transverse localization and slow propagation of light," *Phys. Rev. A* **72**, 021801(R) (2005).
13. M. Vengalattore and M. Prentiss, "Radial confinement of light in an ultracold anisotropic medium," *Phys. Rev. Lett.* **95**, 243601 (2005).

14. D. Tarhan, N. Postacioglu, and Özgür E. Müstecaplioglu, “Ultraslow optical waveguiding in an atomic bose-einstein condensate,” *Opt. Lett.* **32**, 1038–1040 (2007).
15. T. Hong, “Spatial weak-light solitons in an electromagnetically induced nonlinear waveguide,” *Phys. Rev. Lett.* **90**, 183901 (2003).
16. I. Friedler, G. Kurizki, O. Cohen, and M. Segev, “Spatial Thirring-type solitons via electromagnetically induced transparency,” *Opt. Lett.* **30**, 3374–3376 (2005).
17. C. Gómez-Reino and E. Larrea, “Paraxial imaging and transforming in a medium with gradient-index: transmittance function,” *Appl. Opt.* **21**, 4271 (1982).
18. L. Zhang and J. Evers, “Diffractionless image propagation and frequency conversion via four-wave mixing exploiting the thermal motion of atoms,” *Phys. Rev. A* **89**, 013817 (2014).
19. R. Y. Chiao, P. L. Kelley, and E. Garmire, “Stimulated four-photon interaction and its influence on stimulated rayleigh-wing scattering,” *Phys. Rev. Lett.* **17**, 1158–1161 (1966).
20. R. L. Carman, R. Y. Chiao, and P. L. Kelley, “Observation of degenerate stimulated four-photon interaction and four-wave parametric amplification,” *Phys. Rev. Lett.* **17**, 1281–1283 (1966).
21. R. W. Boyd, M. G. Raymer, P. Narum, and D. J. Harter, “Four-wave parametric interactions in a strongly driven two-level system,” *Phys. Rev. A* **24**, 411–423 (1981).
22. K.-i. Harada, K. Mori, J. Okuma, N. Hayashi, and M. Mitsunaga, “Parametric amplification in an electromagnetically-induced transparency medium,” *Phys. Rev. A* **78**, 013809 (2008).
23. C. F. McCormick, A. M. Marino, V. Boyer, and P. D. Lett, “Relative-intensity squeezing at audio frequencies using four-wave mixing in an atomic vapor,” arXiv:quant-ph/0703111v1 (2007).
24. V. G. Vaselago, “The electrodynamics of substances with simultaneously negative values of μ and ϵ ,” *Sov. Phys. Usp.* **10**, 509–514 (1968).
25. A. Gavrielides, P. Peterson, and D. Cardimona, “Diffractive imaging in threewave interactions,” *J. Appl. Phys.* **62**, 2640–2645 (1987).
26. W. Happer and B. S. Mathur, “Effective operator formalism in optical pumping,” *Phys. Rev.* **163**, 12–25 (1967).
27. Q. Glorieux, R. Dubessy, S. Guibal, L. Guidoni, J.-P. Likforman, T. Coudreau, and E. Arimondo, “Double-lambda microscopic model for entangled light generation by four-wave mixing,” *Phys. Rev. A* **82**, 033819 (2010).
28. V. Boyer, A. M. Marino, R. C. Pooser, and P. D. Lett, “Entangled images from four-wave mixing,” *Science* **321**, 544–547 (2008).

1. Introduction

The diffraction of light during propagation in free space is a fundamental and generally unavoidable physical phenomenon. Diffracting light beams do not maintain their intensity distribution in the plane transverse to the propagation direction, unless belonging to a particular class of non-diffracting (Bessel) beams [1]. In nonuniform media, waveguiding is possible for specific spatial modes [2, 3], or equivalently arbitrary images may revive after a certain self-imaging distance [4]. However in such waveguides, the suppression of diffraction for multi-mode profiles is not trivial, as each transverse mode propagates with a different propagation constant or group velocity, resulting in spatial dispersion of the profile.

Recently, a mechanism was suggested and demonstrated for manipulating the diffraction of arbitrary images imprinted on a light beam for arbitrary propagation distances [5, 6]. The technique is based on electromagnetically induced transparency (EIT) [7] in a thermal atomic gas. Unlike other methods utilizing EIT [2–4, 8–17], which rely on spatial non-uniformity, this technique prescribes non-uniformity in k_{\perp} space. Here, k_{\perp} denotes the transverse wave vectors, *i.e.*, the Fourier components of the envelope of the field in the transverse plane, which is the natural basis for paraxial diffraction. The technique of Refs. [5, 6] relies on the diffusion of the atoms in the medium and on the resulting diffraction-like optical response. However, the resolution limit of such motional-induced diffraction in currently available experimental conditions is on the order of 100 μm , preventing it from being of much practical use. Higher resolution requires a denser atomic gas, in which strong absorption is unavoidable due to imperfect EIT conditions. Very recently, Zhang and Evers proposed to circumvent the absorption by generalizing the model of motional-induced diffraction to a four-wave mixing (FWM) process in combination with EIT [18]. The FWM process further allows the frequency conversion of the image and increases the available resolution.

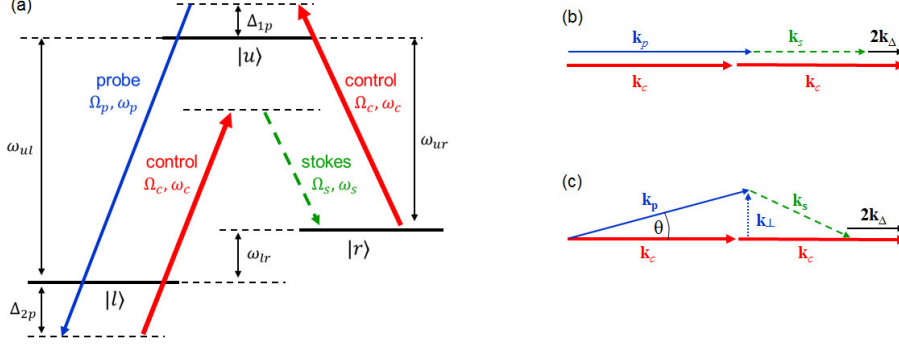


Fig. 1. (a) Four-wave mixing in a three-level Λ system ($|u\rangle$, $|l\rangle$, and $|r\rangle$). Ω_i with $i = c, p, s$ are the Rabi frequencies of the fields. The phase-matching conditions are shown for (b) collinear and (c) non-collinear propagation. The phase mismatch scalar is $2k_\Delta = (2k_c - k_p - k_s) \hat{\mathbf{z}}$.

In this paper, we propose a scheme to manipulate diffraction using FWM [19–21] *without* the need for motional-induced diffraction. The mechanism we study originates from phase matching in k_\perp space and does not require a gaseous medium; it is therefore directly applicable to solid nonlinear media. For our model to be general and to accommodate motional-broadening mechanisms (not important in solids), we here still concentrate on describing atomic gases and validate our model against relevant experiments. The inherent gain of the FWM process allows us to improve the spatial resolution by working with relatively higher gas densities while avoiding loss due to absorption.

In Sec. 2, we introduce a microscopic model of FWM in a Λ system, based on Liouville-Maxwell equations, similar to the one used in Ref. [22]. In Sec. 3, we compare the model to recent experimental results of FWM in hot vapor [22, 23]. We use our model in Sec. 4 to show that, with specific choice of frequencies, the k_\perp dependency of the FWM process can be used to eliminate the diffraction of a propagating light beam. We also present a demonstration of negative diffraction, implementing a paraxial version of a negative-index lens [24], similar to the one in Ref. [6] but with positive gain and higher resolution. Finally, we analyze the resolution limitation of our scheme and propose ways to enhance it. We show that, for cold atoms at high densities ($\sim 10^{12} \text{ cm}^{-3}$), diffraction-less propagation of an image with a resolution of $\sim 10 \mu\text{m}$ can be achieved.

2. Theory

2.1. Model

We consider an ensemble of three-level atoms in a Λ configuration depicted in Fig. 1a. The atomic states are denoted as $|u\rangle$, $|l\rangle$, and $|r\rangle$, for the up, left, and right states, and the optical transition frequencies ω_{ul} and ω_{ur} are assumed to be much larger than the ground-state splitting $\omega_{lr} = \omega_{ul} - \omega_{ur}$. The atom interacts with a weak 'probe' and two 'control' electromagnetic fields, propagating in time t and space \mathbf{r} ,

$$\begin{aligned}
 \mathbf{E}_{cl}(\mathbf{r}, t) &= (\hbar/\mu) \boldsymbol{\varepsilon}_{cl} \Omega_c(\mathbf{r}, t) e^{-i\omega_c t} e^{ik_0^c z}, \\
 \mathbf{E}_{cr}(\mathbf{r}, t) &= (\hbar/\mu) \boldsymbol{\varepsilon}_{cr} \Omega_c(\mathbf{r}, t) e^{-i\omega_c t} e^{ik_0^c z}, \\
 \mathbf{E}_p(\mathbf{r}, t) &= (\hbar/\mu) \boldsymbol{\varepsilon}_p \Omega_p(\mathbf{r}, t) e^{-i\omega_p t} e^{ik_0^p z}.
 \end{aligned} \tag{1}$$

To simplify the formalism, the same dipole moment is assumed for the two optical transitions $\mu = \mu_{ul} = \mu_{ur}$, and the two control fields differ only in their polarizations. Here ω_i are the frequencies of the 'probe' ($i = p$) and the 'control' fields ($i = c$); $k_0^i \equiv \omega_i/c$ are the wave vectors in the case of plane waves, otherwise they are carrier wave-vectors; and $\Omega_i(\mathbf{r}, t)$ are the slowly varying envelopes of the the Rabi frequencies, satisfying $|\partial_t^2 \Omega_i(\mathbf{r}, t)| \ll |\omega_i \partial_t \Omega_i(\mathbf{r}, t)|$ and $|\partial_z^2 \Omega_i(\mathbf{r}, t)| \ll |k_i^0 \partial_z \Omega_i(\mathbf{r}, t)|$. The polarization vectors of the fields are $\boldsymbol{\varepsilon}_p$, $\boldsymbol{\varepsilon}_{cl}$, and $\boldsymbol{\varepsilon}_{cr}$. The strong control and weak probe fields stimulate a weak classical 'Stokes' field (or 'conjugate') at a frequency $\omega_s = 2\omega_c - \omega_p$,

$$\mathbf{E}_s(\mathbf{r}, t) = (\hbar/\mu)\boldsymbol{\varepsilon}_s\Omega_s(\mathbf{r}, t)e^{-i\omega_s t}e^{ik_0^s z}. \quad (2)$$

To further simplify the analysis, we assume a single relaxation rate Γ between the excited and ground levels and define the complex rates $\gamma_{cr} = \Gamma - i(\omega_c - \omega_{ur})$ and $\gamma_{cl} = \Gamma - i(\omega_c - \omega_{ul})$ for each of the optical transitions. Within the ground state, we consider a population relaxation with symmetric rates $\Gamma_{l \leftrightarrow r}$ and a decoherence with a rate Γ_{lr} . In a frame rotating with the control frequency ω_c , the equations of motion for the local density-matrix $\rho(\mathbf{r}, t)$ are better written in terms of the slowly-varying density-matrix $R(\mathbf{r}, t)$, where $R_{u,j}(\mathbf{r}, t) = \rho_{u,j}(\mathbf{r}, t)e^{i\omega_c t - ik_0^c z}$ for $j = l, r$ and $R_{\alpha, \alpha'}(\mathbf{r}, t) = \rho_{\alpha, \alpha'}(\mathbf{r}, t)$ for all other matrix elements,

$$\begin{aligned} \frac{\partial}{\partial t} R_{l,l} &= -2\text{Im}(\hat{P}^* R_{u,l}) + \Gamma_{l \leftrightarrow r}(R_{r,r} - R_{l,l}) + \Gamma R_{u,u} \\ \frac{\partial}{\partial t} R_{r,r} &= -2\text{Im}(\hat{S}^* R_{u,r}) - \Gamma_{l \leftrightarrow r}(R_{r,r} - R_{l,l}) + \Gamma R_{u,u} \\ \frac{\partial}{\partial t} R_{u,u} &= 2\text{Im}(\hat{P}^* R_{u,l}) + 2\text{Im}(\hat{S}^* R_{u,r}) - 2\Gamma R_{u,u} \\ \frac{\partial}{\partial t} R_{r,l} &= i\hat{S}^* R_{u,l} - i\hat{P} R_{u,r}^* - (\Gamma_{lr} + i\omega_{lr})R_{r,l} \\ \frac{\partial}{\partial t} R_{u,l} &= -i\hat{P}(R_{u,u} - R_{l,l}) + i\hat{S} R_{r,l} + \gamma_{cl}^* R_{u,l} \\ \frac{\partial}{\partial t} R_{u,r} &= -i\hat{S}(R_{u,u} - R_{r,r}) + i\hat{P} R_{r,l}^* + \gamma_{cr}^* R_{u,r}. \end{aligned} \quad (3)$$

Here

$$\hat{P} \equiv \Omega_p(\mathbf{r}, t)e^{-i(\delta_\omega t - \delta_k z)} + \Omega_c \quad \text{and} \quad \hat{S} \equiv \Omega_s(\mathbf{r}, t)e^{i(\delta_\omega t - \delta_k z)} + \Omega_c \quad (4)$$

are interference fields, and $\delta_\omega = \omega_p - \omega_c = \omega_c - \omega_s$ and $\delta_k = k_0^p - k_0^c = k_0^c - k_0^s$ are detuning parameters.

Finally assuming non-depleted control fields, constant in time and space $\Omega_c(\mathbf{r}, t) = \Omega_c$, we complete the description of the atom-field interaction with the propagation equations under the envelope approximation for the probe field

$$\left(\frac{\partial}{\partial z} + \frac{1}{c} \frac{\partial}{\partial t} + \frac{i\nabla_\perp^2}{2q} \right) \Omega_p(\mathbf{r}, t) = igR_{u,l}(\mathbf{r}, t)e^{i(\delta_\omega t - \delta_k z)} \quad (5a)$$

and the Stokes field

$$\left(\frac{\partial}{\partial z} + \frac{1}{c} \frac{\partial}{\partial t} - \frac{i\nabla_\perp^2}{2q} \right) \Omega_s(\mathbf{r}, t) = igR_{u,r}(\mathbf{r}, t)e^{-i(\delta_\omega t - \delta_k z)}, \quad (5b)$$

where $\nabla_\perp^2 \equiv \partial^2/\partial x^2 + \partial^2/\partial y^2$ the transverse Laplacian, $g = 2\pi N|\mu|^2 q/\hbar$ the coupling strength proportional to the atomic density N , and $q \equiv |k_0^c| \approx |k_0^p| \approx |k_0^s|$. To obtain Eqs. (5b), we neglected the second-order t and z derivatives of the envelopes.

2.2. Steady-state solution

The evolution of the fields is described by a set of non-linear, coupled differential equations for the density matrix elements $R_{\alpha,\alpha'}$ and the weak fields Ω_p and Ω_s [Eqs. (3)-(5b)], which require further approximations in order to be solved analytically. Most importantly, we assume the proximity to two-photon resonance, such that δ_ω is on the order of the ground-state frequency splitting ω_{lr} and much larger than any detuning, Rabi frequency, or pumping rate in the system. Other assumptions are detailed in the appendix, where we derive the steady state of the system to first order in the weak fields,

$$R_{\alpha,\alpha'} \simeq R_{\alpha,\alpha'}^{(0)} + R_{\alpha,\alpha'}^{(1)}, \quad (6)$$

with $R_{\alpha,\alpha'}^{(0)}$ and $R_{\alpha,\alpha'}^{(1)}$ being the zero- and first- order steady-state solutions. Plugging Eqs. (23)-(26) and (6) for $R_{u,r}$ and $R_{u,l}$ into the propagation equations (5b) and discarding terms rotating at δ_ω and $2\delta_\omega$, we obtain the well-known FWM form including paraxial diffraction,

$$\left(\frac{\partial}{\partial z} - i \frac{1}{2q} \nabla_\perp^2 \right) \Omega_p(\mathbf{r}) = A \Omega_p(\mathbf{r}) + B \Omega_s^*(\mathbf{r}), \quad (7a)$$

$$\left(\frac{\partial}{\partial z} + i \frac{1}{2q} \nabla_\perp^2 \right) \Omega_s^*(\mathbf{r}) = C \Omega_p(\mathbf{r}) + D \Omega_s^*(\mathbf{r}), \quad (7b)$$

where

$$A \equiv -\alpha_p + \frac{\beta_p}{\gamma_{pl}\gamma_0} |\Omega_c|^2, \quad B \equiv \frac{\beta_s}{\gamma_{pl}\gamma_0} |\Omega_c|^2, \quad (8)$$

$$C \equiv \frac{\beta_p}{\gamma_{sr}^*\gamma_0} |\Omega_c|^2, \quad D \equiv -\alpha_s^* + \frac{\beta_s}{\gamma_{sr}^*\gamma_0} |\Omega_c|^2.$$

Here $\alpha_j = g(n_l/\gamma_{jl} + n_r/\gamma_{jr})$ are the linear absorption coefficients of the probe ($j = p$) or Stokes ($j = s$) fields, with $n_i \equiv R_{i,i}^{(0)}$ the populations of the $i = r, l$ levels. $\beta_p = g(n_l/\gamma_{pl} + n_r/\gamma_{cr}^*)$ and $\beta_s = g(n_r/\gamma_{sr}^* + n_l/\gamma_{cl})$ are two-photon interaction coefficients, $\gamma_{jk} = \Gamma - i(\omega_j - \omega_{uk})$ [$j = p, c, s; k = l, r$] are complex one-photon detunings, and $\gamma_0 = \Gamma_{lr} + |\Omega_c|^2/\gamma_{sr}^* + |\Omega_c|^2/\gamma_{pl} - i(\delta_\omega - \omega_{lr})$ is the complex two-photon detuning. Eqs. (7) are similar to those obtained by Harada *et al.* [22] but here including the diffraction term $\pm i \nabla_\perp^2 / (2q)$, required to explore the spatial evolution of the fields.

We start with the simple case of a weak plane-wave probe $\Omega_p(\mathbf{r}) = f(z) e^{ik_\perp^p \cdot r_\perp} e^{i(k_z^p - k_0^p)z}$ directed at some small angle $\theta \approx k_\perp^p/k_0^p \ll 1$ relatively to the z axis (Fig. 1). The generated Stokes field is then also a plane wave $\Omega_s(\mathbf{r}) = g(z) e^{ik_\perp^s \cdot r_\perp} e^{i(k_z^s - k_0^s)z}$. Substituting into Eqs. (7), the phase-matching condition $\vec{k}_\perp^s = -\vec{k}_\perp^p$ is readily obtained, and the resulting equations for f and g are [21]

$$f'(z) = A f(z) + B g^*(z) e^{i2k_\Delta z} \quad \text{and} \quad g'(z) = C f(z) e^{-i2k_\Delta z} + D g^*(z), \quad (9)$$

where $2k_\Delta = (2k^c - k^p - k^s) \cdot \hat{z} \approx k_\perp^2/q$ is the phase mismatch scalar [see Figs. 1(b) and (c)].

Assuming $f(0) = 1$ and $g(0) = 0$, we follow Ref. [21] and find along the medium

$$f(z) e^{-ik_\Delta z} = \frac{A - \lambda_2}{\lambda_1 - \lambda_2} e^{\lambda_1 z} - \frac{A - \lambda_1}{\lambda_1 - \lambda_2} e^{\lambda_2 z}, \quad (10a)$$

$$g^*(z) e^{ik_\Delta z} = -\frac{C}{\lambda_1 - \lambda_2} \left(e^{\lambda_1 z} - e^{\lambda_2 z} \right), \quad (10b)$$

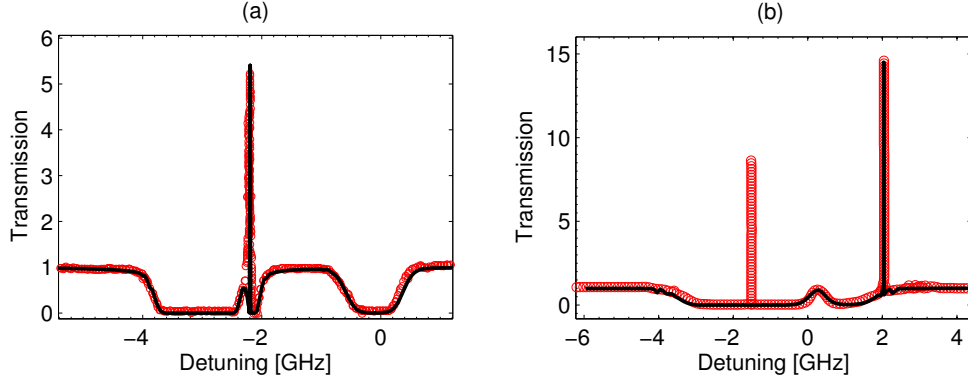


Fig. 2. Transmission spectra of FWM in (a) rubidium vapor and (b) sodium vapor for a weak probe as a function of the two-photon detuning. The red circles are experimental data from (a) Ref. [23] and (b) Ref. [22]. The black line is calculated from Eqs. (10)-(11) with the following parameters. For the rubidium experiment: $\omega_{lr} = -3$ GHz, $\Gamma_{rl} = 5$ MHz, $\Omega_c = 165$ MHz, $\Gamma = 5.7$ MHz, $N = 1.9 \times 10^{12}$ cm $^{-3}$, $\Delta_{1p} = \omega_c - \omega_{ur} = 0.8$ GHz, $L = 12.5$ mm, $T = 150^\circ$ C, and $k_{\perp}/q = 5.2$ mrad. For the sodium experiment: $\omega_{lr} = 1.777$ GHz, $\Gamma_{rl} = 1$ MHz, $\Omega_c = 45$ MHz, Γ MHz, $N = 4.4 \times 10^{11}$ cm $^{-3}$, $\Delta_{1p} = \omega_c - \omega_{ur} = 2$ GHz, $L = 45$ mm, $T = 165^\circ$ C, $k_{\perp}/q = 4.5$ mrad.

with the eigenvalues $\lambda_{1,2} = (A + D)/2 \pm [(A - D - i2k_{\Delta})^2/4 + BC]^{1/2}$. A similar analysis for the case of three-wave mixing was presented by Gavrielides *et al.* [25].

In the limit where $|B|$ and $|C|$ are much smaller than $|A|$ and $|D|$, the solution is governed by independent EIT for the probe and Stokes fields with little coupling between them. In the opposite limit, the fields experience strong coupling, and the real part of the eigenvalues $\lambda_{1,2}$ can be made positive and result in gain.

3. Comparison with experiments

To verify our model, we have calculated the probe transmission as a function of the two-photon detuning and compared it to the data published in Refs. [22, 23]. The Doppler effect due to the motion of the thermal atoms is taken into account by averaging the FWM coefficients, $Q = A, B, C, D$ in Eq. (8), over the Doppler profile [26]. Assuming nearly collinear beams, the mean coefficients are

$$\bar{Q} = \frac{1}{\sqrt{2\pi}v_{th}} \int du Q(\omega_p + qu, \omega_c + qu) \exp\left(\frac{-u^2}{2v_{th}^2}\right), \quad (11)$$

where $v_{th} = k_B T/m$, T the cell temperature, and m the atomic mass.

Figure 2 shows the transmission spectrum in (a) rubidium vapor and (b) sodium vapor (cells length $L \simeq 5$ cm). Here and in what follows, we characterize the resonance conditions by the one-photon detuning $\Delta_{1p} = \omega_c - \omega_{ur}$ and the two-photon detuning $\Delta_{2p} = \omega_p - \omega_c - \omega_{lr}$ (see Fig. 1a). Our model reproduces the experimental spectra, including the Doppler-broadened absorption lines and the gain peaks for both rubidium and sodium experiments. The missing peak in Fig. 2b is due to anti-Stokes generation not included in the model.

4. Diffraction manipulation by FWM

We now concentrate on a specific choice of frequency detunings, for which the phase dependency of the FWM process can be used to manipulate the diffraction of the propagating probe

and Stokes. To this end, we study the evolution of an arbitrary image $F(r)$ imprinted on the probe beam, with the boundary conditions $\Omega_p(r_\perp, 0) = F(r)$ and $\Omega_s(r_\perp, 0) = 0$. Our prime examples shall be the propagation of the image *without diffraction* or with *reverse diffraction*, both of which while experiencing gain.

4.1. Image propagation

We start by solving Eqs. (7) in the transverse Fourier basis,

$$\left(\frac{\partial}{\partial z} + i\frac{k_\perp^2}{2q} - \bar{A}\right)\Omega_p(k_\perp, z) = \bar{B}\Omega_s^*(k_\perp, z), \quad (12a)$$

$$\left(\frac{\partial}{\partial z} - i\frac{k_\perp^2}{2q} - \bar{D}\right)\Omega_s^*(k_\perp, z) = \bar{C}\Omega_p(k_\perp, z), \quad (12b)$$

where $\Omega_{p/s}(k_\perp, z) = \int dr_\perp^2 e^{-ik_\perp \cdot r_\perp} \Omega_{p/s}(r_\perp, z)$, and the coefficients \bar{A} , \bar{B} , \bar{C} , and \bar{D} are Doppler averaged according to Eq. (11). We notice that Eqs. (12) are identical to Eqs. (9) with $k_\Delta = 0$ and with the substitutions $\bar{A} \rightarrow \bar{A} - ik_\perp^2/(2q)$ and $\bar{D} \rightarrow \bar{D} + ik_\perp^2/(2q)$. The evolution of the probe and Stokes fields then follows from Eq. (10),

$$\frac{\Omega_p(k_\perp, z)}{\Omega_p(k_\perp, 0)} = \frac{\bar{A} - ik_\perp^2/q - \lambda_2}{\lambda_1 - \lambda_2} e^{\lambda_1 z} - \frac{\bar{A} - ik_\perp^2/q - \lambda_1}{\lambda_1 - \lambda_2} e^{\lambda_2 z}, \quad (13a)$$

$$\frac{\Omega_s(k_\perp, z)}{\Omega_p(k_\perp, 0)} = \frac{-\bar{C}}{\lambda_1 - \lambda_2} (e^{\lambda_1 z} - e^{\lambda_2 z}), \quad (13b)$$

where

$$\lambda_{1,2} = \frac{\bar{A} + \bar{D}}{2} \pm \frac{1}{2} \sqrt{(\bar{A} - \bar{D} - i\frac{k_\perp^2}{q})^2 + 4\bar{B}\bar{C}}. \quad (14)$$

We choose $|e^{\lambda_2 z}| \gg |e^{\lambda_1 z}|$ and obtain $\Omega_p(k_\perp, z) = \Omega_p(k_\perp, 0) e^Z$, where

$$Z \equiv \lambda_2 z + \log\left(\frac{\bar{A} - ik_\perp^2/q - \lambda_1}{\lambda_2 - \lambda_1}\right) \quad (15)$$

determines the changes in the spatial shape of the probe along its propagation. $\text{Re}Z$ is responsible for the k_\perp -dependency of the gain/absorption, and $\text{Im}Z$ is responsible for the k_\perp -dependency of the phase accumulation, that is, the diffraction-like evolution.

4.2. Suppression of paraxial diffraction

In general, the minimization of both the real and the imaginary k_\perp -dependencies of Z is required in order to minimize the distortion of the probe beam. To better understand the behavior of Z , we expand it in orders of k_\perp^2 . Taking the limit

$$k_\perp^2 \ll k_0^2 = \min\left(\frac{2qE^2}{\bar{A} - \bar{D}}, 2qE\right), \quad (16)$$

where $2E = [(\bar{A} - \bar{D})^2 + 4\bar{B}\bar{C}]^{1/2}$, we write

$$Z \approx Z^{(0)} + \frac{k_\perp^2}{2q} Z^{(2)} + O(k_\perp^4) \quad (17)$$

and find

$$Z^{(0)} \approx \left(\frac{\bar{A} + \bar{D}}{2} - E\right) z, \quad Z^{(2)} = i\left(\frac{\bar{A} - \bar{D}}{2E} z + \frac{\bar{A} - \bar{D}}{2E^2} - \frac{1}{E}\right). \quad (18)$$

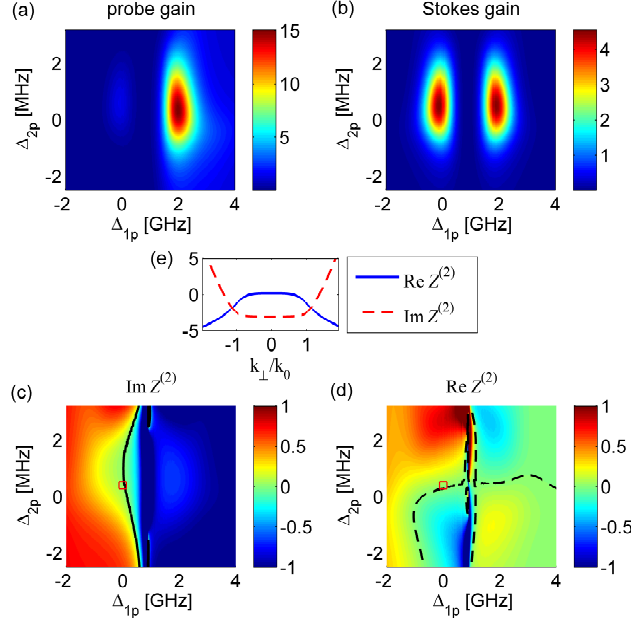


Fig. 3. Numerical search for the detuning values that yield suppression of paraxial diffraction and positive gain. This example uses the conditions of the sodium system in Fig. 2. The colormaps as a function of the one- and two-photon detunings are: (a) the Probe’s gain, (b) Stokes’ gain, (c) $\text{Im}Z^{(2)}$ of Eq. (18), and (d) $\text{Re}Z^{(2)}$. The contour $\text{Im}Z^{(2)} = 0$ is plotted in solid line in (c). The contour $\text{Re}Z^{(2)} = 0$ is plotted in dashed line in (d). (e) The exact propagation-exponent Z [Eq. (15)] for the case $\Delta_{2p} \approx 0.4$ MHz and $\Delta_{1p} \approx 0$ [red square in (c) and (d)]. At these detunings, $\text{Re}Z^{(2)} = \text{Im}Z^{(2)} = 0$, and both the real and imaginary parts of Z are constant for $k_{\perp} \ll k_0 = 40 \text{ mm}^{-1}$.

The k_{\perp} -dependency, governed by $Z^{(2)}$, can be controlled through the FWM coefficients \bar{A} , \bar{B} , \bar{C} , and \bar{D} given in Eq. (8), by manipulating the frequencies of the probe and control fields (ω_p , ω_c), the control amplitude Ω_c , and the density N .

We demonstrate this procedure in Fig. 3, using for example the experimental conditions of the sodium experiment, detailed in Fig. 2. First, we observe the gain of the probe and the Stokes fields in Fig. 3a and 3b, as a function of the one- (Δ_{1p}) and two- (Δ_{2p}) photon detunings. The gain is achieved around the two-photon resonance ($\Delta_{2p} \approx 0$), either when the probe is at the one-photon resonance ($\Delta_{1p} \approx 0$) or the Stokes ($\Delta_{1p} \approx \omega_{lr}$, here ≈ 2 GHz); the latter exhibits higher gain, since the probe sits outside its own absorption line. The real and imaginary parts of $Z^{(2)}$ are plotted in Figs. 3c and 3d. When $\text{Re}Z^{(2)} = 0$ (dashed line), the gain/absorption is not k_{\perp} -dependent, whereas when $\text{Im}Z^{(2)} = 0$ (solid line), the phase accumulation along the cell is not k_{\perp} -dependent. When both happen, $Z^{(2)} = 0$, and a probe with a spectrum confined within the resolution limit $k_{\perp} \ll k_0$ propagates without distortion. The exact propagation exponent Z as a function of k_{\perp} for the point $Z^{(2)} = 0$ ($\Delta_{2p} \approx 0.4$ MHz, $\Delta_{1p} \approx 0$) are plotted in Fig. 3e. As expected, both real (blue solid line) and imaginary (red dashed line) parts of Z are constant for $k_{\perp} \ll k_0$ (deviation of 1% within $k_{\perp} < k_0/2$ and 0.1% within $k_{\perp} < k_0/4$). In the specific example of Fig. 3, the probe’s gain is ~ 1.4 , the Stokes’ gain is ~ 4 , and $k_0 \approx 40 \text{ mm}^{-1}$.

To illustrate the achievable resolution, we shall employ a conservative definition for a characteristic feature size in the image in area units $a = (2\pi/k_{\perp})^2$ [For example: for a Gaussian

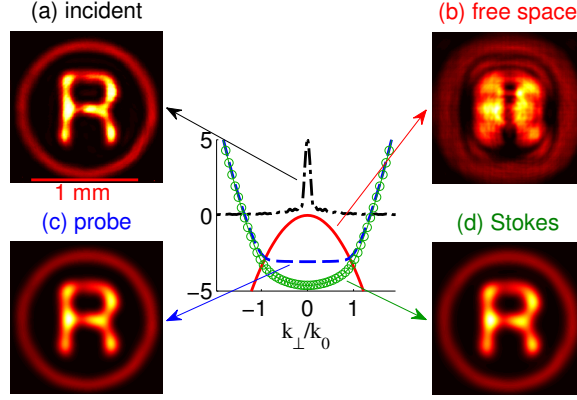


Fig. 4. Simulations demonstrating the suppression of paraxial diffraction by FWM. (a) incident image, (b) after propagating in free space, (c) probe image after propagating in the FWM medium, and (d) generated Stokes image. The diffraction terms of the Probe (blue dashed line) and Stokes (green circles) fields are compared with free-space diffraction (red line). The k_{\perp} spectrum of the image is given for comparison (black dash-dot line). The probe propagates in the cell with very little diffraction, and the Stokes' distortion due to diffraction is reduced. The calculation is carried out in the conditions highlighted in Fig. 3 (detunings $\Delta_{2p} = 0.4$ MHz and $\Delta_{1p} = 0$ and other parameters as in Fig. 2b). The image is about 1-mm wide (features area 0.025 mm^2) and the propagation distance 45 mm (equivalent to $\lesssim 2$ Rayleigh lengths).

beam, $a^{1/2}$ shall be twice the waist radius, and, for the field pattern $E = 1 + \cos(k_{\perp x}) \cos(k_{\perp y})$, the pixel area is a^2 . The Rayleigh length is $qa^2/8$. Fig. 4 presents numerical calculations of Eqs. (13) in the conditions found above for a probe beam in the shape of the symbol (R) with features of $a \approx 0.025 \text{ mm}^2$ (corresponding to $k_{\perp} = k_0 = 40 \text{ mm}^{-1}$). The propagation distance is $L = 45 \text{ mm}$, equivalent to $\lesssim 2$ Rayleigh distances as evident by the substantial free-space diffraction. Indeed when $Z^{(2)} = 0$, the FWM medium dramatically reduces the distortion of the image due to diffraction. Note that the image spectrum (black dashed-dotted line) lies barely within the resolution limit and that the Stokes distortion due to diffraction is also reduced. We emphasize that direct numerical solutions of Eqs. (7) give exactly the same results. For the hot sodium system, the required control-field intensity is on the order of 100 mW for beams with a waist radius of a few mm, which is practically a plane wave on the length scale of the image.

4.3. Negative paraxial diffraction

Another interesting application of diffraction manipulation is imaging by negative diffraction, similar to the one proposed in Ref. [6]. Using the same tools as above, one can find the conditions for the reversal of paraxial diffraction, namely when $\text{Re}Z^{(2)}$ vanishes and $\text{Im}Z^{(2)} = 1$ (free space diffraction is equivalent to $Z^{(2)} = -i$).

At these conditions, as demonstrated in Fig. 5, the FWM medium of length L focuses the radiation from a point source at a distance $u < L$ to a distance v behind the cell, where $u + v = L$. The mechanism is simple: each k_{\perp} component of the probe accumulates outside the cell the phase $-ik_{\perp}^2(u + v)/(2q) = -ik_{\perp}^2 L/(2q)$ and inside the cell the phase $ik_{\perp}^2 L/(2q)$, summing up to zero phase accumulation. The probe image thus 'revives', with some additional gain, at the exit face of the cell.

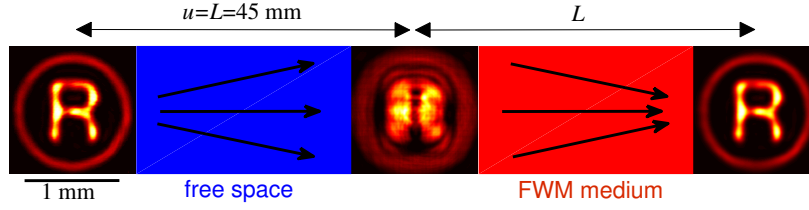


Fig. 5. Demonstration of paraxial lensing with FWM. The negative-diffraction medium of length L focuses an image located at a distance $u < L$ to a distance v behind the cell, where $u + v = L$. In this example, $u = L = 45$ mm and $v = 0$. The probe gain is 1.5. The parameters (for which $Z^{(2)} = i$) are $\Delta_{2p} = 0.4$ MHz, $\Delta_{1p} = -1.7$ GHz, and $N = 4 \times 10^{12}$ cm $^{-3}$; other parameters are as detailed in Fig. 2b.

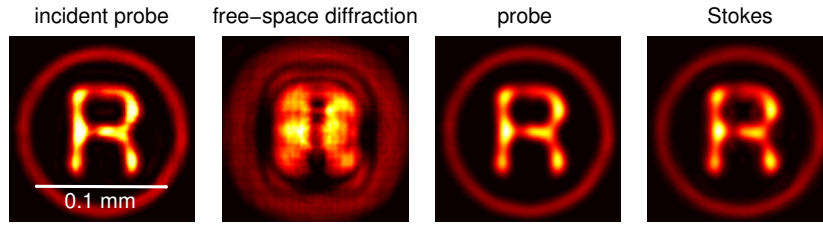


Fig. 6. Calculations for cold sodium atoms at a density of $N = 10^{12}$ cm $^{-3}$ and negligible Doppler broadening. The image size is 0.1 mm with 10- μ m features. The propagation distance is 0.45 mm (~ 1.5 Rayleigh length).

5. Conclusions and discussion

The suggested mechanism for manipulating the paraxial diffraction of light utilizes the k_{\perp} -dependency of the four-wave mixing process and is thus fundamentally different than that suppressing the diffraction of spatial solitons in nonlinear media. The inherent gain of the FWM process allows one to take advantage of high optical-depths while avoiding absorption and, by that, achieving higher resolution than with previous EIT-based schemes [5, 6]. As oppose to a recent proposal incorporating FWM [18], our scheme does not require atomic motion and is expected to work even more efficiently in its absence. We have introduced a microscopic model for the FWM process, based on Liouville-Maxwell equations and incorporating Doppler broadening, and verified it against recent experimental results. The conditions for which the FWM process suppresses the paraxial diffraction were delineated. We have demonstrated the flexibility of the scheme to surpass the regular diffraction and reverse it, yielding an imaging effect while introducing gain. Our proposal was designed with the experimental limitations in mind, and its demonstration should be feasible in many existing setups.

The resolution limit $a^{-1} \propto k_0^2$ of our scheme (and thus the number of 'pixels' S/a for a given beam area S) is proportional to the resonant optical depth. In practice, the latter can be increased either with higher atomic density N or narrower optical transitions. For example, using a density of $N = 5 \cdot 10^{12}$ cm $^{-3}$, 10 times higher than in the sodium setup of Ref. [22], the limiting feature area would be 250 μ m 2 ($k_0 \approx 125$ mm $^{-1}$). As long as $NL = const$, the other parameters required for the suppression of diffraction remain the same. At the same time, the reduced Doppler broadening in cold atoms media and in solids would substantially increase the resolution limit. Assuming cold atoms with practically no Doppler broadening (and ground-state

relaxation rate $\Gamma_{lr} = 100$ Hz), the same limiting feature of $250 \mu\text{m}^2$ can be obtained at a reasonable density of 10^{12} cm^{-3} . Finally, we note that the best conditions for suppression of diffraction are not always achieved by optimizing $Z^{(2)}$ alone (first order in k_{\perp}^2/k_0^2); In some cases, one could improve significantly by working with higher orders. As demonstrated in Fig. 6, combining the aforementioned methods for resolution enhancement with $N = 10^{12} \text{ cm}^{-3}$ cold atoms, a resolution-limited feature area as low as $100 \mu\text{m}^2$ with unity gain can be achieved. Going beyond this resolution towards the $1 - 10 \mu\text{m}^2$ -scale for microscopy applications requires the lifting of the paraxial assumption in the analysis.

The FWM process conserves quantum coherence on the level of single photons, as was shown theoretically [27] and experimentally [28] by measuring spatial coherence (correlation) between the outgoing probe and Stokes beams. An intriguing extension of our work would thus be into the single-photon regime. Specifically, the main limitation in the experiment of Ref. [28] was the trade-off between focusing the beams to the smallest spot possible while keeping the 'image' from diffracting throughout the medium. Our scheme circumvents this trade-off by maintaining the fine features of the image for much larger distances.

Acknowledgments

We thank O. Peleg and J. Evers for helpful discussions.

Appendix: Steady-state solution

Assuming control fields constant in time and space and much stronger than the probe and Stokes fields, the steady-state solution of Eqs. (3)-(5b) can be approximated to lowest orders in the weak fields as $R_{\alpha,\alpha'} \simeq R_{\alpha,\alpha'}^{(0)} + R_{\alpha,\alpha'}^{(1)}$, where $R_{\alpha,\alpha'}^{(0)}$ is the zero-order and $R_{\alpha,\alpha'}^{(1)}$ the first-order steady-state solutions. We find $R_{\alpha,\alpha'}^{(0)}$ from the zero-order equations of motion

$$\begin{aligned}
\frac{\partial}{\partial t} R_{l,l}^{(0)} &= -2 \text{Im}(\Omega_c^* R_{u,l}^{(0)}) + \Gamma R_{u,u}^{(0)} + \Gamma_{l \leftrightarrow r} (R_{r,r}^{(0)} - R_{l,l}^{(0)}) \\
\frac{\partial}{\partial t} R_{r,r}^{(0)} &= -2 \text{Im}(\Omega_c^* R_{u,r}^{(0)}) + \Gamma R_{u,u}^{(0)} - \Gamma_{l \leftrightarrow r} (R_{r,r}^{(0)} - R_{l,l}^{(0)}) \\
\frac{\partial}{\partial t} R_{u,u}^{(0)} &= 2 \text{Im}(\Omega_c^* R_{u,l}^{(0)}) + 2 \text{Im}(\Omega_c^* R_{u,r}^{(0)}) - 2\Gamma R_{u,u}^{(0)} \\
\frac{\partial}{\partial t} R_{r,l}^{(0)} &= i\Omega_c^* R_{u,l}^{(0)} - i\Omega_c R_{u,r}^{(0)} - i\omega_{lr} R_{r,l}^{(0)} - \Gamma_{lr} R_{r,l}^{(0)} \\
\frac{\partial}{\partial t} R_{u,l}^{(0)} &= -i\Omega_c (R_{u,u}^{(0)} - R_{l,l}^{(0)}) + i\Omega_c R_{r,l}^{(0)} + \gamma_{cl} R_{u,l}^{(0)} \\
\frac{\partial}{\partial t} R_{u,r}^{(0)} &= -i\Omega_c (R_{u,u}^{(0)} - R_{r,r}^{(0)}) + i\Omega_c R_{r,l}^{(0)} + \gamma_{cr} R_{u,r}^{(0)}
\end{aligned} \tag{19}$$

by solving $(\partial/\partial t)R_{\alpha,\alpha'}^{(0)} = 0$. Under the assumption $|\Omega_c/\omega_{lr}| \ll 1$, thus $R_{r,l}^{(0)} = 0$, we obtain for the other elements

$$\begin{aligned}
R_{l,l}^{(0)} &= \frac{2A_r A_l + \Gamma A_r + \Gamma_{l\leftrightarrow r}(A_l + A_r + \Gamma)}{X} \\
R_{r,r}^{(0)} &= \frac{2A_r A_l + \Gamma A_l + \Gamma_{l\leftrightarrow r}(A_l + A_r + \Gamma)}{X} \\
R_{u,u}^{(0)} &= \frac{2A_r A_l + \Gamma_{1\leftrightarrow 2} A_r + \Gamma_{l\leftrightarrow r} A_l}{X} \\
R_{u,l}^{(0)} &= i \frac{\Omega_c \Gamma (\Gamma_{1\leftrightarrow 2} + A_r)}{\gamma_{cl} X} \\
R_{u,r}^{(0)} &= i \frac{\Omega_c \Gamma (\Gamma_{1\leftrightarrow 2} + A_l)}{\gamma_{cr} X}, \tag{20}
\end{aligned}$$

with the denominator

$$X = 6A_r A_l + 2\Gamma_{l\leftrightarrow r} \Gamma + A_r (3\Gamma_{l\leftrightarrow r} + \Gamma) + A_l (3\Gamma_{l\leftrightarrow r} + \Gamma), \tag{21}$$

and $A_{l/r} = |\Omega_c|^2 \text{Im}[(\omega_{ul/ur} - \omega_c - i\Gamma)^{-1}]$ the optical pumping rates.

To find $R_{\alpha,\alpha'}^{(1)}$, we start from the first-order equations of motion,

$$\begin{aligned}
\frac{\partial}{\partial t} R_{l,l}^{(1)} &= -2 \text{Im} \left[\Omega_p^* e^{-i\delta_k z + i\delta_{\omega t}} R_{u,l}^{(0)} + \Omega_c^* R_{u,l}^{(1)} \right] - (\Gamma - \Gamma_{l\leftrightarrow r}) R_{r,r}^{(1)} - (\Gamma + \Gamma_{l\leftrightarrow r}) R_{l,l}^{(1)} \\
\frac{\partial}{\partial t} R_{r,r}^{(1)} &= -2 \text{Im} \left[\Omega_s^* e^{i\delta_k z - i\delta_{\omega t}} R_{u,r}^{(0)} + \Omega_c^* R_{u,r}^{(1)} \right] - (\Gamma + \Gamma_{l\leftrightarrow r}) R_{r,r}^{(1)} - (\Gamma - \Gamma_{l\leftrightarrow r}) R_{l,l}^{(1)} \\
\frac{\partial}{\partial t} R_{r,l}^{(1)} &= i(\Omega_s^* R_{u,l}^{(0)} - \Omega_p R_{u,r}^{(0)}) e^{i\delta_k z - i\delta_{\omega t}} + i\Omega_c^* R_{u,l}^{(1)} - i\Omega_c R_{u,r}^{(1)} - i(\omega_{lr} - i\Gamma_{lr}) R_{r,l}^{(1)} \\
\frac{\partial}{\partial t} R_{u,l}^{(1)} &= -i\Omega_p e^{i\delta_k z - i\delta_{\omega t}} (R_{u,u}^{(0)} - R_{l,l}^{(0)}) + i\Omega_c (R_{r,r}^{(1)} + 2R_{l,l}^{(1)} + R_{r,l}^{(1)}) - \gamma_{cl} R_{u,l}^{(1)} \\
\frac{\partial}{\partial t} R_{u,r}^{(1)} &= -i\Omega_s e^{-i\delta_k z + i\delta_{\omega t}} (R_{u,u}^{(0)} - R_{r,r}^{(0)}) + i\Omega_c (R_{l,l}^{(1)} + 2R_{r,r}^{(1)} + R_{r,l}^{(1)}) - \gamma_{cr} R_{u,r}^{(1)}. \tag{22}
\end{aligned}$$

Eqs. (22) are explicitly time-dependent, and we cannot directly solve for $(\partial/\partial t)R_{\alpha,\alpha'}^{(1)} = 0$.

Instead, we introduce the new variables $P_{\alpha,\alpha'}^{(1)}$ and $N_{\alpha,\alpha'}^{(1)}$ and rewrite Eqs. (22) using

$$R_{\alpha,\alpha'}^{(1)} = P_{\alpha,\alpha'}^{(1)} e^{i[\delta_{\omega t} - \delta_k z]} + N_{\alpha,\alpha'}^{(1)} e^{-i[\delta_{\omega t} - \delta_k z]}, \tag{23}$$

eliminating the explicit dependency on time. The steady-state solution is obtained from the complete set of linear algebraic equations for the variables $P_{u,l}^{(1)}, P_{u,r}^{(1)}, P_{r,l}^{(1)}, N_{u,l}^{(1)}, N_{u,r}^{(1)}, N_{r,l}^{(1)}$,

$P_{l,l}^{(1)}$, and $P_{r,r}^{(1)}$,

$$\begin{aligned}
0 &= \Omega_c^* P_{u,l}^{(1)} - \Omega_c N_{u,l}^{*(1)} + \Omega_p^* R_{u,l}^{(0)} + i(\Gamma - \Gamma_{l \leftrightarrow r}) P_{r,r}^{(1)} + (i\Gamma + i\Gamma_{l \leftrightarrow r} - \delta_\omega) P_{l,l}^{(1)} \\
0 &= \Omega_c^* P_{u,r}^{(1)} - \Omega_c N_{u,r}^{*(1)} - \Omega_s R_{u,r}^{*(0)} + (i\Gamma + i\Gamma_{l \leftrightarrow r} - \delta_\omega) P_{r,r}^{(1)} + i(\Gamma - \Gamma_{l \leftrightarrow r}) P_{l,l}^{(1)} \\
0 &= \Omega_c^* P_{u,l}^{(1)} - \Omega_c N_{u,r}^{*(1)} - (\omega_{lr} - i\Gamma_{lr} + \delta_\omega) P_{r,l}^{(1)} \\
0 &= \Omega_c N_{u,l}^{*(1)} - \Omega_c^* P_{u,r}^{(1)} - (\omega_{lr} + i\Gamma_{lr} - \delta_\omega) N_{r,l}^{*(1)} - \Omega_p^* R_{u,r}^{(0)} + \Omega_s R_{u,l}^{*(0)} \\
0 &= \Omega_c (P_{r,r}^{(1)} + 2P_{l,l}^{(1)} + P_{r,l}^{(1)}) + (i\gamma_{cl} + \delta_\omega) P_{u,l}^{(1)} \\
0 &= \Omega_c^* (P_{r,r}^{(1)} + 2P_{l,l}^{(1)} + N_{r,l}^{*(1)}) + (i\gamma_{cl}^* + \delta_\omega) N_{u,l}^{*(1)} - \Omega_{p,l}^* (R_{u,u}^{(0)} - R_{l,l}^{(0)}) \\
0 &= \Omega_c^* (P_{l,l}^{(1)} + 2P_{r,r}^{(1)} + P_{r,l}^{(1)}) - (i\gamma_{cr}^* - \delta_\omega) N_{u,r}^{*(1)} \\
0 &= \Omega_c (P_{l,l}^{(1)} + 2P_{r,r}^{(1)} + N_{r,l}^{*(1)}) - (i\gamma_{cr} - \delta_\omega) P_{u,r}^{(1)} + \Omega_{s,r} (R_{u,u}^{(0)} - R_{r,r}^{(0)})
\end{aligned} \tag{24}$$

The exact solution of Eqs. (24) is easily obtained but is unmanageable and bears no physical intuition. Rather, we derive an approximate solution under the following assumptions:

1. The control and probe frequencies are near two-photon resonance, $|\Delta_{2p}| = |\delta_\omega - \omega_{lr}| \ll \omega_{lr}$.
2. The ground-state population relaxation is much slower than the excited-to-ground relaxation, $\Gamma_{r \leftrightarrow l} \ll \Gamma$.
3. The optical pumping is much slower than the ground-state frequency difference $\Omega_c^2/\Gamma \ll \omega_{lr}$.

Under these assumptions, and taking the control Rabi frequency to be real $\Omega_c = \Omega_c^*$, we solve Eqs. (24) and obtain the coherences relevant to the evolution of the probe and the Stokes [Eqs. (5b)],

$$iN_{u,l}^{(1)} = \left(\frac{n_l}{\gamma_{pl}} + \frac{n_r}{\gamma_{cr}} - \frac{n_l/\gamma_{pl} + n_r/\gamma_{cr}^*}{\gamma_{pl}\gamma_0} \Omega_c^2 \right) \Omega_p + \frac{n_r/\gamma_{sr}^* + n_l/\gamma_{cl}}{\gamma_{pl}\gamma_0} \Omega_c^2 \Omega_s^*, \tag{25}$$

$$iP_{u,r}^{(1)} = \left(\frac{n_r}{\gamma_{sr}} + \frac{n_l}{\gamma_{cl}} - \frac{n_r/\gamma_{sr} + n_l/\gamma_{cl}^*}{\gamma_{sr}\gamma_0^*} \Omega_c^2 \right) \Omega_p + \frac{n_l/\gamma_{pl}^* + n_r/\gamma_{cr}}{\gamma_{sr}\gamma_0^*} \Omega_c^2 \Omega_p^*. \tag{26}$$